

Adaptive Bayesian Changepoint Analysis & Local Outlier Scoring

Haoxuan Wu and David S. Matteson

October 30, 2021

Abstract

We introduce global-local shrinkage priors into a Bayesian dynamic linear model to adaptively estimate both changepoints and local outliers in a novel model we call Adaptive Bayesian Changepoints with Outliers (ABCO). We utilize a state-space approach to identify a dynamic signal in the presence of outliers and measurement error with stochastic volatility. We find that global state equation parameters are inadequate for most real applications and we include local parameters to track noise at each time-step. This setup provides a flexible framework to detect unspecified changepoints in complex series, such as those with large interruptions in local trends, with robustness to outliers and heteroskedastic noise. ABCO may also be used as a robust Bayesian trend filter that can reconstruct interrupted time series. We further detail the extension of our approach to time-varying parameter estimation within dynamic regression analysis to identify structural breaks. Finally, we compare our algorithm against several alternatives to demonstrate its efficacy in diverse simulation scenarios and two empirical examples.¹

1 Introduction

Changepoint analysis involves detecting changes in the distribution of a time series. The prevalence of larger data sets is accompanied by increased complexity and decreased homogeneity (Rehman *et al.*, 2016). We aim to understand how the underlying distribution of a time series changes, to distinguish unspecified local trends from major changes, and to do so in the presence of stochastic volatility and outliers. Change point analysis has a wide variety of applications: in genetics, it is used to identify changes within DNA sequences (Braun *et al.*, 2000); in environmental science, it is applied to quantify climate change (Solow, 1987); in finance, it helps gain insights into historical data and improves future forecasting (Chen and Gupta, 1997); in EEG analysis, it identifies key signals for monitoring health status of patients (Chen *et al.*, 2019). The flexible and adaptive framework we propose can extend the application of changepoint analysis to even more domains of research.

¹Financial support is gratefully acknowledged from a Xerox PARC Faculty Research Award, National Science Foundation Awards 1455172, 1934985, 1940124, and 1940276, USAID, and Cornell University Atkinson Center for a Sustainable Future.

Many approaches have been used to identify changepoints. One approach considers the changepoint problem as anomaly detection (Aminikhanghahi and Cook, 2017). Another approach is to apply a distance-based metric, such as cumulative sum (Cho and Fryzlewicz, 2015), energy distance (Matteson and James, 2014) and Kullback-divergence (Liu *et al.*, 2013), to segment a series into contiguous clusters. Identifying breaks within state-space models has also been proposed (Kawahara *et al.*, 2007). While these approaches can prove effective in detecting the locations of changepoints, they have limited flexibility and do not typically provide uncertainty quantification.

From the Bayesian perspective, changepoints can broadly be considered locations that partition data into contiguous clusters generated from different probability distributions (Adams and MacKay, 2007). Recursive Bayesian inversion paired with importance sampling can be applied to analyze the probability of a sequence coming from a common probability distribution (Tan *et al.*, 2015). However, this, and many other approaches, makes the strong assumption that observations within each segment are independent and identically distributed (iid), which greatly limits the scope of suitable applications.

Several machine learning approaches, including recurrent neural network (Ebrahimbzadeh *et al.*, 2019), Gaussian process (Saatçi *et al.*, 2010), and Hidden Markov Models (Montanez *et al.*, 2015), have been utilized for changepoint analysis. Such approaches can demonstrate extreme flexibility, but many lack robustness or are “black-box” in nature, lacking interpretability. They typically require large training series, expert structural specification and hyper-parameter selection.

Nearly all existing changepoint algorithms are unreliable in the presence of unlabeled outliers or heteroskedastic noise. Outliers significantly change distributional estimates and tend to violate the commonly required Gaussian noise assumption of algorithms. To specifically address changepoint analysis in the presence of outliers, Fearnhead and Rigaill (2017) proposed an alternative biweight loss function to cap the influence of individual observations. While successful, the algorithm is sensitive to regularization parameters for both the influence threshold and the number of change points, which are difficult to specify in practice. Giordani *et al.* (2007) proposed a state-space framework that incorporates thresholding for modeling smooth transitions and Markov switching for modeling outliers. While also successful, this method lacks robustness to noisy data, over-segmenting heteroskedastic series in high volatility periods.

In this paper, we propose a new method called Adaptive Bayesian Changepoints with Outliers (ABCO). At its core, ABCO utilizes a threshold autoregressive stochastic volatility model within a time-varying parameter model to estimate smoothly varying trends with large, isolated interruptions. Through a state-space framework, ABCO successfully models heteroskedastic measurement errors, and identifies both local outliers and change points jointly. Utilizing several efficient sampling techniques, ABCO is also computationally efficient, with complexity $\mathcal{O}(\mathcal{T})$ for a length T series. Within the observation equation, we decompose a series into three basic components: a locally varying trend signal, a sparse additive outlier signal, and a heteroskedastic noise process. Our specification allows locally

adaptive modeling for both trend and variability, automatically adjusting to periods of high and low volatility.

ABCO’s trend modeling extends the Bayesian trend filter approach of [Kowal *et al.* \(2019\)](#) to include interruptions and the detection of changepoints. Local smoothing is accomplished by specifying first or second order differences in the trend process as sparse signals through global-local shrinkage priors ([Carvalho *et al.*, 2009](#)). To diminish insignificant patterns and merge sustained trends together, while still allowing instantaneous changes, we specify a local shrinkage “process” prior through a threshold stochastic volatility model, with appropriately distributed innovations. A threshold parameter establishes a self-correcting mechanism that penalizes the occurrence of consecutive changepoints within short intervals. This also allows for posterior inference of changepoint locations and size. This is all performed while also accounting for additive outliers, which we specify with an ultra sparse horseshoe+ prior [Bhadra *et al.* \(2017\)](#). Finally, by combining locally estimated outlier and noise parameters we also define a posterior local outlier score for labeling each observation as likely anomalous, or not.

Our paper proceeds as follows. Section 2 details ABCO and our novel use of horseshoe priors. Section 3 contrasts ABCO with many alternative methods, including a basic horseshoe approach, PELT ([Killick *et al.*, 2012](#)), E.Divisive ([Matteson and James, 2014](#); [Zhang *et al.*, 2019](#)), Wild Binary Segmentation (WBS, [Fryzlewicz, 2014](#)), and Bayesian changepoint analysis (BCP, [Erdman and Emerson, 2008](#)), in diverse simulation scenarios. Section 4 investigates two real world applications using ABCO. Section 5 concludes, with discussion of future extensions.

2 Methodology

ABCO decomposes a time series $\{y_t\}$ into three components: a local mean or trend signal $\{\beta_t\}$, a sparse additive outlier signal $\{\zeta_t\}$ and a heteroskedastic noise process $\{\epsilon_t\}$, as simply

$$y_t = \beta_t + \zeta_t + \epsilon_t, \quad \epsilon_t \sim N(0, \sigma_{\epsilon t}^2), \quad (1)$$

where $\epsilon_t = \varepsilon_t \sigma_{\epsilon t}$ and $\varepsilon_t \stackrel{iid}{\sim} N(0, 1)$. ABCO’s decomposition effectively distinguishes a potentially locally varying mean or trend signal from a complex error process $\{\zeta_t + \epsilon_t\}$ that may contain outliers and exhibit volatility clustering. Next, we detail each of the three model components of ABCO.

We assume the noise process $\{\sigma_{\epsilon t}^2\}$ follows a stochastic volatility (SV) model to capture potential heteroskedasticity. For simplicity, we focus on the first order [SV(1)] model of ([Kim *et al.*, 1998](#)) with Gaussian innovations in log volatility. Specifically, we assume

$$\log(\sigma_{\epsilon t}^2) = \mu_\epsilon + \phi_\epsilon [\log(\sigma_{\epsilon, t-1}^2) - \mu_\epsilon] + \xi_{\epsilon t}, \quad \xi_{\epsilon t} \sim N(0, \sigma_\xi^2).$$

We find this relatively simple noise model to be adequate in practice, but more complex specifications are also easily substituted into ABCO for specific applications.

By modeling observational noise using an SV(1) model, we concisely account for heteroskedastic measurement error. By supposing $\sigma_{\epsilon t}^2$ is a constant σ_ϵ^2 for all t , we have measurement error with constant variance, which we later denote as ABCO w/o SV. As shown in Sections 3 and 4, including stochastic volatility greatly improves detection of changes in series with noise variance changes, including random or slowly varying, while maintaining an equal level of performance in series with constant noise variance, with minimal computational cost. This simple modeling component has not been widely adopted in other change point models; it provides ABCO with enhanced flexibility for modeling more varied and complex applications.

2.1 Local Outlier Detection and Scoring

The sparse outlier process $\{\zeta_t\}$ models large deviations at specific times, for which we suppose an independent horseshoe+ shrinkage prior, as in [Bhadra *et al.* \(2017\)](#):

$$\begin{aligned} (\zeta_t | \lambda_{\zeta t}, \tau_\zeta, \eta_{\zeta t}) &\sim N(0, \lambda_{\zeta t}^2), & \tau_\zeta &\sim C^+(0, \sigma_{\tau_\zeta}), \\ (\lambda_{\zeta t} | \tau_\zeta, \eta_{\zeta t}) &\sim C^+(0, \tau_\zeta \eta_{\zeta t}), & \eta_{\zeta t} &\sim C^+(0, \sigma_{\eta_\zeta}), \end{aligned}$$

where $C^+(\cdot)$ denotes the half-Cauchy distribution, and σ_{τ_ζ} and σ_{η_ζ} are hyper-parameters controlling the global and local prior shrinkage of outliers, respectively. The process $\{\zeta_t\}$ concentrates near zero except at locations where deviations from the mean trend also strongly deviate from nearby residuals in magnitude. As such, we call it a sparse outlier process, and although outliers may cluster, they are assumed independent *a priori* by this specification.

Applying a horseshoe prior provides appropriate shrinkage, pushing $\{\zeta_t\}$ toward either zero or a very large value. However, as we generally define outliers to be rare in occurrence we desire $\{\zeta_t\}$ to rarely take values outside a tight neighborhood of zero, and this requires a even stronger shrinkage than the horseshoe provides. The alternative horseshoe+, with the additional term $\{\eta_{\zeta,t}\}$, provides more extreme horseshoe shaped shrinkage, and allows only a few values to largely deviate from zero.

In order identify specific observations y_t as potential or likely outliers, we propose a locally adaptive outlier score o_t based on the proportion of conditional variance attributed to the outlier component ζ_t relative to the variance of the overall error $\zeta_t + \epsilon_t$. From observation Equation (1) and the additional specification details discussed earlier, we note $\text{Var}(y_t | \beta_t, \lambda_{\zeta t}, \sigma_{\epsilon t}) = \lambda_{\zeta t}^2 + \sigma_{\epsilon t}^2$; i.e. conditional on the local trend β_t , variability is split between the outlier and heteroskedastic noise terms. We thus propose the following observational outlier score, using M posterior samples (with MCMC implementation details discussed later), as: $o_t = \frac{1}{M} \sum_{i=1}^M \frac{\lambda_{\zeta t}^{2(i)}}{\lambda_{\zeta t}^{2(i)} + \sigma_{\epsilon t}^{2(i)}}$ where $(\lambda_{\zeta t}^{2(i)}, \sigma_{\epsilon t}^{2(i)})$ denotes the i th posterior draw of

$(\lambda_{\zeta_t}^2, \sigma_{\epsilon t}^2)$. Outlier scoring provides a single ordering of the observations with respect to their relative local deviations. We apply these scores to shade the most locally anomalous observation points in later figures. Thresholding these (temporally) marginal outlier scores is a simple approach to labeling locally outlying points, and comprehensive joint analysis of outlier scores is a promising future research direction.

2.2 Trend Filtering with Changepoints

The local mean or trend signal $\{\beta_t\}$ is specified as our primary state variable. To model a local trend we focus on modeling increments in β_t , e.g., $\Delta^D \beta_t$, where Δ^D is the D th difference operator (usually for D equal to 1 or 2), with priors that induce sparsity. We suppose the following model

$$\begin{aligned} \Delta^D \beta_t &= \omega_t, & h_t &= \log(\tau_\omega^2 \lambda_{\omega t}^2), \\ \omega_t &\sim N(0, \tau_\omega^2 \lambda_{\omega t}^2), & h_t &= \mu + (\phi_1 + \phi_2 s_t)(h_{t-1} - \mu) + \eta_t, \end{aligned} \quad (2)$$

where s_t is defined below and $\eta_t \stackrel{iid}{\sim} Z(\alpha, \beta, 0, 1)$, in which Z denotes the four parameter Z -distribution, and (α, β) are hyperparameters which we fix as $(\frac{1}{2}, \frac{1}{2})$ for simplicity, see [Kowal et al. \(2019\)](#).

In Equation 3 the trend increments, i.e. the evolution error $\{\omega_t\}$, is modeled by a global-local shrinkage prior with parameters τ_ω and $\{\lambda_{\omega t}\}$. The global parameter τ_ω establishes the overall evolution error scale while the local parameters $\{\lambda_{\omega t}\}$ shrink evolution errors locally with respect to time. Previous work introduced a simple first order stochastic volatility SV(1) model for the process $\{\omega_t\}$ through a first order autoregression of $\{h_t\}$ with Z -distributed innovations, and showed it produced exceptionally flexible shrinkage appropriate for adaptive trend filtering ([Kowal et al., 2019](#)).

To now allow trend filtering with abrupt breaks, i.e. isolated changepoints, we consider a similarly simple, but more flexible stochastic volatility model for $\{\omega_t\}$, a first order *threshold* stochastic volatility TSV(1) model. This is equivalent to specifying a first order threshold autoregression for $\{h_t\}$, again with Z -distributed innovations. The proposed TSV(1) model appears in Equation 3 above, in which the zero-one threshold indicator process $\{s_t\}$ allows the volatility model to exhibit an asymmetric response, ϕ_1 versus $\phi_1 + \phi_2$, in h_t with respect to a threshold variable, which we specify as $\log(\omega_t^2)$. Specifically, for a threshold parameter γ we define

$$s_t = 1 \text{ if } \log(\omega_t^2) > \gamma, \quad \text{and } 0 \text{ otherwise.}$$

Through a SV(1) prior with Z -distributed innovations, the posterior shrinkage profile for $\{\omega_t\}$ will tend to swing between extended periods of extreme shrinkage, in which ω_t is estimated as approximately zero, and periods of less or minimal shrinkage, in which ω_t is volatile and hence the trend β_t itself is dynamically evolving. In the presence of isolated change points in the signal β_t , which coincide with

large values of $\log(\omega_t^2)$, h_t is pushed higher. When ϕ_1 is closer to one than zero, the process h_t also remains higher for several periods, because of the persistence induced by strong short-term memory in the autoregression. When now applying a TSV(1) prior, with the threshold indicator s_t is added, and with $\phi_2 < 0$, the process $\{h_t\}$ can immediately return to a lower level following a large value of $\log(\omega_t^2)$. Overall, use of the proposed TSV(1) specification avoids over-estimation of change points, especially in high volatility periods.

In Equation (3), if we fix $\phi_1 = \phi_2 = 0$, we have non-dynamic shrinkage, in that $\{\lambda_{\omega t}\}$ is iid, and we refer to this special case the ‘horseshoe’ evolution model, or simply horseshoe in this paper as it applies the standard horseshoe prior for the evolution error variance. In Section 3 below we compare the performance of ABCO with the horseshoe model above, and several other popular approaches, in a comprehensive simulation study. And in Appendix 6.2 we illustrate the further use of ABCO to estimate changepoints within the parameters of a dynamic regression.

2.3 Interrupted Time Series

Interrupted time series analysis refers to the study of time series in which a known event or intervention has taken effect at a specific time; the goal of the analysis is to compare the pre-intervention period series with the post-intervention period series to assess the nature and impact of the intervention. For an interrupted time series $\{\dots, y_{\pi-1}, y_\pi, \dots\}$ where an intervention commenced at time index π , a traditional linear interrupted time series model can be written as follows ([Wagner et al., 2002](#)):

$$y_t = \alpha_0 + \alpha_1 t + \alpha_2 I_t^\pi + \alpha_3(t - \pi + 1)I_t^\pi + e_t,$$

where α_0 and α_1 are the intercept and slope of the time trend regression pre-intervention; I_t^π is an indicator variable noting whether the time index t occurs pre-intervention ($I_t^\pi = 0$ for all $t < \pi$) or post-intervention ($I_t^\pi = 1$ for all $t \geq \pi$); α_2 is the intervention effect with respect to any level shift; and α_3 is the intervention effect associated with any change in slope after intervention. Furthermore, the noise term e_t is most commonly assumed to be iid (or autoregressive), and normally distributed with mean 0 and variance σ_e^2 . This relatively simple traditional interrupted time series model has proven broadly applicable in analyzing effect of intervention in medication use research ([Wagner et al., 2002](#)), public health policy ([Bernal et al., 2017](#)) and performance based incentives ([Serumaga et al., 2011](#)).

ABCO can be easily adapted to apply to an interrupted time series, but with more flexibility than a traditional approach. Explicit modeling of both outliers and heteroskedastic noise (around the intervention time in particular) is achieved through maintaining the same observation decomposition $y_t = \beta_t + \zeta_t + \epsilon_t$, and specifications for $\{\zeta_t\}$ and $\{\epsilon_t\}$. ABCO’s flexible trend modeling allows general nonlinear trends before and after intervention. Furthermore, ABCO allow for a more detailed

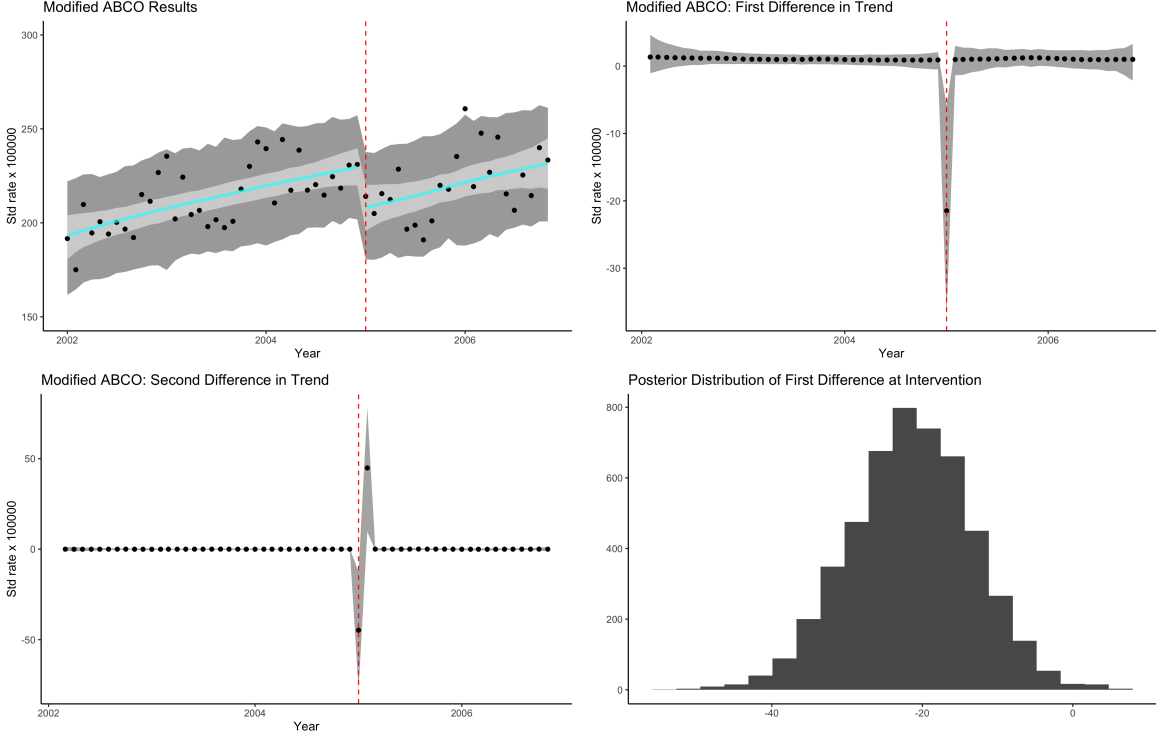
characterization of the intervention effect beyond an abrupt change in level and/or slope at time π . This might include anticipatory interventions effects or an intervention effect that resulted in only a temporary change. Now, to assess the impact of an intervention of the form above, i.e. level and/or slope changes at time π , we focus on modeling second order ($D = 2$) changes in $\{\beta_t\}$ and modify the ABCO state increment equation as follows:

$$\begin{aligned} \Delta^2\beta_t &= \omega_t + v_t, & v_\pi, v_{\pi+1} &\sim N(0, \sigma_v^2), \\ \omega_t &\sim N(0, \tau_\omega^2 \lambda_{\omega t}^2), & v_t &= 0 \quad \text{otherwise,} \end{aligned} \quad (3)$$

where σ_v^2 is assumed to be sufficiently large to give v_π and $v_{\pi+1}$ a relatively diffuse prior. Note that we expect an intervention effect to induce a large value for $|\Delta\beta_\pi|$, and in the general case of a level and/or slope change at π a large value for $|\Delta^2\beta_\pi|$, as well as potentially for $|\Delta^2\beta_{\pi+1}|$, is expected. Thus the terms v_π and $v_{\pi+1}$ are added to allow for corresponding changes in the underlying trend, while the same ABCO $\{\omega_t\}$ process as introduced in Section 2.2 above is applied. The interpretation of ABCO now extends to include an abrupt disruption at time π in a trend that is otherwise estimated to be approximately linear locally. The magnitude of the break or change in both level and slope after the intervention specified as a function of v_π and $v_{\pi+1}$. This and related modifications of ABCO are specifically used for series with one (or more) interruptions at one (or more, but well separated) intervention times.

For a simple illustration of applying ABCO to an interrupted time series follows we consider the effect of a smoking ban in Sicily, Italy on the hospital admission rate for acute coronary events (ACE) (Barone-Adesi *et al.*, 2011). Monthly ACE rate is recorded from 2002 to 2006 with a smoking ban taking place January of 2005. The dataset has been previously analyzed using interrupted time series in Bernal *et al.* (2017). The series is shown in Figure 1, with the results of applying the modified ABCO method. The most prominent feature is a major level shift in the underlying trend after the smoking ban in January of 2005, but the slope (rate of increase over time) before and after the intervention appears very similar. Our overall conclusions in this case are very similar to the finding of traditional interrupted time series analysis (Bernal *et al.*, 2017). Some of the advantages the modified ABCO provides is flexibility in estimating the trends pre- and post-intervention; robustness to any outliers or heteroskedastic noise; adaptive uncertainty quantification over time and at the intervention time in particular. We note from the figure that there is roughly constant variability in changes in the trend (although slightly larger post intervention) except at time π where ABCO has estimated substantially more uncertainty about the intervention effect size. This is highlighted in the right panel which shows the estimated posterior distribution for $\Delta\beta_\pi$ which is centered around -20, but with substantial variability. Additional standard model checking was performed but not shown.

Figure 1: Effect of Smoking Ban on Rate of Acute Coronary Events in Sicily, Italy



The top-left panel shows the standardized rate of ACE over time, with the estimated modified ABCO model for interrupted time series. The posterior mean trend for $\{\beta_t\}$ is shown in cyan along with 95% credible bands for $\{\beta_t\}$ in light gray and 95% credible bands for $\{y_t\}$ in dark gray. The estimated trend appears to be linear before and after the intervention data, with a level shift downward, but with little change in slope. The top-right panel shows the first degree difference in the trend $\{\Delta\beta_t\}$ from the modified ABCO ($\{\Delta^2\beta_t = \omega_t + \nu_t\}$) along with 95% credible bands in dark gray. With the single departure from the otherwise constant increments we have no evidence of anticipatory or temporary intervention effects; the intervention appears to have only had an immediate, but sustained impact, in intercept in this case. The bottom-left panel shows the second degree difference in the trend $\{\Delta\beta_t\}$ from the modified ABCO along with 95% credible bands in dark gray. The negative departure at time π and the positive bounce-back of similar magnitude at time $\pi + 1$ further support idea of a shift in intercept but not in slope at time of intervention. The bottom-right panel shows the posterior distribution of the first difference of $\{\beta_t\}$ at the intervention time π (i.e. $\Delta\beta_\pi$). From here the modified ABCO approach allow model-based inference on the effect size at intervention.

2.4 Inference

We conduct posterior inference via Markov chain Markov Carlo. In particular, we define a Gibbs sampling algorithm which iteratively samples parameters from their full conditional distributions. In this section, we provide an overview of the sampling steps of ABCO. The details for the majority of these components are expanded in Appendix 6.1 as they follow closely from related work (Kowal *et al.*, 2019). The exception is the threshold variable γ , which is more difficult to estimate and sampling details are summarized below.

Let $\mathbf{Y} = [y_1, \dots, y_T]$, $\mathbf{h} = [h_1, \dots, h_T]$, $\boldsymbol{\eta} = [\eta_1, \dots, \eta_T]$, $\boldsymbol{\beta} = [\beta_1, \dots, \beta_T]$, $\boldsymbol{\sigma}_\epsilon^2 = [\sigma_{\epsilon 1}^2, \dots, \sigma_{\epsilon T}^2]$, $\boldsymbol{\zeta} = [\zeta_1, \dots, \zeta_T]$, $\boldsymbol{\lambda}_\zeta = [\lambda_{\zeta 1}, \dots, \lambda_{\zeta T}]$, $\boldsymbol{\eta}_\zeta = [\eta_{\zeta 1}, \dots, \lambda_{\eta T}]$ and $\boldsymbol{\xi}_\epsilon = [\xi_{\epsilon 1}, \dots, \xi_{\epsilon T}]$. Sampling all variables in the evolutionary equation from their full conditional involves sampling the log volatility $p(\mathbf{h}|\boldsymbol{\beta}, \phi_1, \phi_2, \mu, \gamma, \boldsymbol{\eta})$, the unconditional mean $p(\mu|\mathbf{h}, \boldsymbol{\beta}, \phi_1, \phi_2, \gamma, \boldsymbol{\eta})$, the evolution equation coefficients $p(\phi_1|\mathbf{h}, \boldsymbol{\beta}, \phi_2, \mu, \gamma, \boldsymbol{\eta})$, $p(\phi_2|\mathbf{h}, \boldsymbol{\beta}, \phi_1, \mu, \gamma, \boldsymbol{\eta})$, the threshold $p(\gamma|\mathbf{h}, \boldsymbol{\beta}, \phi_1, \phi_2, \mu, \boldsymbol{\eta})$ and the evolution error $p(\boldsymbol{\eta}|\mathbf{h}, \boldsymbol{\beta}, \phi_1, \phi_2, \mu, \gamma)$. The state variable is sampled jointly from $p(\boldsymbol{\beta}|\mathbf{h}, \phi_1, \phi_2, \mu, \gamma, \boldsymbol{\eta}, \boldsymbol{\sigma}_\epsilon^2, \boldsymbol{\zeta}, \mathbf{Y})$. The outlier process is sampled from $p(\boldsymbol{\zeta}|\boldsymbol{\beta}, \boldsymbol{\sigma}_\epsilon^2, \boldsymbol{\lambda}_\zeta, \tau_\zeta, \boldsymbol{\eta}_\zeta, \mathbf{Y})$ along with other associated parameters using a sampler for the horseshoe

prior based on the inverse gamma distribution (Makalic and Schmidt, 2016). And the observational variance is sampled from $p(\sigma_\epsilon^2 | \beta, \zeta, \mu_\epsilon, \phi_\epsilon, \xi_\epsilon, \mathbf{Y})$ along with other associated variables using the stochvol package (Hosszejni and Kastner, 2019).

The update for γ is less straightforward relative to the other parameters above. Following derivations in Nakajima and West (2013), for each time step t , marginalizing over ω_t gives $P(\log(\omega_t^2) > \gamma) = P(\omega_t > e^{\gamma/2}) = 1 - \Phi(\frac{e^{y_t/2}}{\tau \lambda_t})$ where Φ is the CDF for standard normal distribution. From this we see that $\tau, \{\lambda_t\}$ and $\{y_t\}$ play important roles in identifying an appropriate range for γ . However, the full conditional distribution for γ does not have a standard form. Despite this challenge, it's important to learn γ from the data, even in the presence of outliers, because it plays a crucial role in determining the location of the change points. After experimenting with numerous sampling schemes, including slice sampling and Metropolis-Hastings, we find that applying the Griddy Gibbs sampler (Ritter and Tanner, 1992) was both simple and adequate for estimating γ within the ABCO model, allowing one to choose essentially any prior for. We further found that a uniform prior, $\gamma \sim \text{Unif}(\ell_\gamma, u_\gamma)$, worked well provided the range was tailored to the observed data, and we relate the lower and upper limits to the volatility of the D th degree differences of the observations. Specifically, we let $\ell_\gamma = \min\{\log[(\Delta^D y_t)^2]\}$ and $u_\gamma = \max\{\log[(\Delta^D y_t)^2]\}$.

2.5 Shrinkage Profile of ABCO

As detailed above, ABCO decomposes observations y_t into three components, $(\beta_t, \zeta_t, \epsilon_t)$, i.e. trend, outlier, and noise components, respectively. Conditional on the noise and outlier components, a horseshoe like shrinkage prior is placed on the variance of the D th degree difference of the trend component. In particular, a threshold stochastic volatility model (THSV) of order 1 with Z -distributed innovations is used to model the log of the variance for the trend component increments. Without the threshold variable $\{s_t\}$ and coefficient ϕ_2 in the model, the shrinkage on $\{\beta_t\}$ follows the dynamic shrinkage process introduced in Kowal *et al.* (2019), wherein the authors detailed its shrinkage profile. Below we discuss and relate the shrinkage profile induced by the state increment variance $\{\tau^2 \lambda_t^2\}$ of ABCO with the dynamic shrinkage process.

Remark 1. Let $\kappa_t = (1 + \tau^2 \lambda_t^2)^{-1}$ denote the shrinkage proportion at time t , where as $\kappa_t \rightarrow 0$ there is no shrinkage and as $\kappa_t \rightarrow 1$ there is maximal shrinkage. The following properties hold for the shrinkage of the trend component in ABCO: Let $\psi_t = (\tau^2)^{(1-\phi_1-\phi_2 s_t)} (\frac{1-\kappa_t}{\kappa_t})^{\phi_1+\phi_2 s_t}$;

- (i) For any $\epsilon \in (0, 1)$, $P(\kappa_{t+1} > 1 - \epsilon | y_{t+1}, \{\kappa_s\}_{s \leq t}, s_t, \phi_1, \phi_2, \tau) \rightarrow 0$ as $\psi_t \rightarrow 0$ uniformly in $y_{t+1} \in \mathbb{R}$;
- (ii) For any $\epsilon \in (0, 1)$ and $\psi_t < 1$, $P(\kappa_{t+1} < \epsilon | y_{t+1}, \{\kappa_s\}_{s \leq t}, s_t, \phi_1, \phi_2, \tau) \rightarrow 1$ as $|y_{t+1}| \rightarrow \infty$.

The proof for both properties can be derived analogously to the proof of Theorem 3 in Kowal *et al.* 2019. The first property notes that ABCO will shrink the variance of the state equation toward 0 as $\tau \rightarrow 0$, confirming τ^2 is a global shrinkage parameter in ABCO. The second property notes that a

sufficiently extreme value of y_{t+1} will still lead to a large change in the underlying mean trend, and this also motivates the use of the outlier process $\{\zeta_t\}$ to redistribute such an extreme, particularly when it is isolated.

Finally, comparing the dynamic shrinkage process with ABCO, we can see that the posterior for κ_{t+1} can be written as

$$[\kappa_{t+1}|y_{t+1}, \{\kappa_s\}_{s \leq t}, s_t, \phi_1, \phi_2, \tau] = (1 - \kappa_{t+1})^{-1/2} [1 + (\psi_t - 1)\kappa_{t+1}]^{-1} \exp(-y_{t+1}^2 \kappa_{t+1}/2).$$

Assuming all other parameters are fixed, the posterior distribution of κ_{t+1} given $s_t = 1$ has more mass near 0 in comparison to the posterior distribution of κ_{t+1} given $s_t = 0$. This further highlights the purpose of the threshold variable; $\{s_t\}$ (and ϕ_2) lowers the shrinkage value of κ_{t+1} after the occurrence of a change point. In this way, ABCO separates isolated jumps in the trend from sustained periods of evolution in the trend.

3 Simulation Experiments

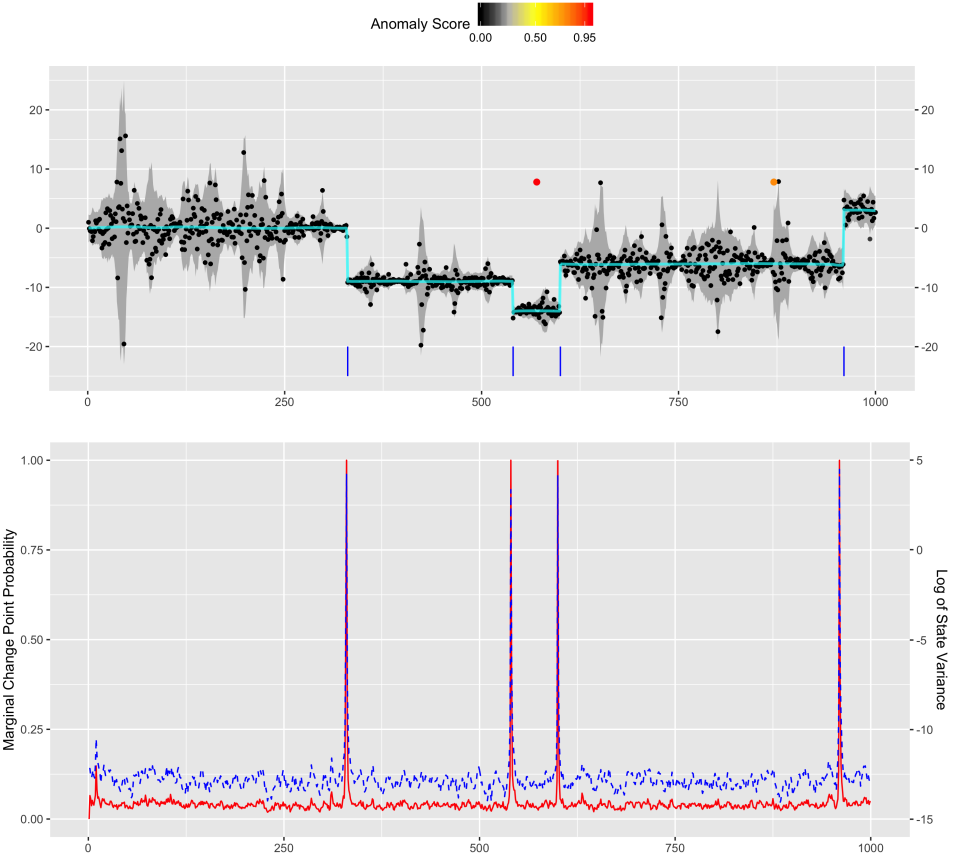
3.1 Multiple Changes in Mean with Heteroskedastic Noise

First, we consider the effectiveness of ABCO in the challenging setting of estimating multiple change-points in mean in the presence of heteroskedastic noise. In this section we generate $N = 100$ simulated series of length $T = 1000$. For each series, the number of change points are generated uniformly at random from the set $\{2, 3, 4\}$. Change point locations are uniformly sampled but with the constraint that their minimal distance is 30 time increments. The resulting segments are each assigned a mean uniformly distributed between -100 and 100. Finally, innovations with stochastic volatility are added to the mean signals, with log volatility specified as

$$\log(\sigma_{\epsilon t}^2) = \phi_\epsilon \log(\sigma_{\epsilon, t-1}^2) + \alpha_t, \quad \alpha_t \sim N(0, \sigma_\alpha^2), \quad (4)$$

with $\phi_\epsilon = 0.9$ and $\sigma_\alpha^2 = 0.6^2$. Figure 2 give an example of such a generated series, but with two outliers also included for illustration here (outliers are considered further below). Each series tends to have substantial local fluctuations which make change point analysis difficult. Table 1 details results comparing the performance of ABCO with the previously mentioned static Horseshoe approach, PELT (Killick *et al.*, 2012), WBS (Fryzlewicz, 2014), E.Divisive (James and Matteson, 2014), and BCP (Erdman and Emerson, 2008). E.Divisive, PELT and WBS are specified using default parameters with minimum segment length 30, and BCP is specified using default parameters, 5000 MCMC iterations, and with change points identified at times indices with posterior probability of a change point above 0.5).

Figure 2: Example Plots for Changes in Mean with Stochastic Volatility



The top plot shows an example of the simulated data with two added outliers (colored in red and orange). The anomaly scoring shows local adaptive of the algorithm; the first outlier (far from high volatility region) has the highest score while the second outlier (near high volatility region) has a slightly lower score. The cyan lines indicate posterior mean of $\{\beta_t\}$; vertical blue lines indicate predicted change points and gray bands indicate 95% point-wise credible bands for the data excluding the anomaly component. The bottom plot shows the marginal probability being a change point at each time step (red line) and $\{\log(\omega_t^2)\}$ (blue dashed line); the marginal probability at each time step t is calculated from the percentage of posterior simulations for $\log(\omega_t^2)$ that exceed the change point threshold r . We can see, as a result of the threshold variable, $\{\log(\omega_t^2)\}$ spikes when change point is predicted and comes down right-away; this is key for not over-predicting in regions of high-volatility.

Results are shown in Table 1, and we can see that the ABCO outperforms the competing models in this scenario. ABCO achieves the highest average Rand value, 0.958, and the highest adjusted Rand average of 0.912, with standard errors of 0.009 and 0.018, respectively. The static Horseshoe approach was a far second based on these metrics, with an average adjusted Rand of 0.528 (se 0.032); others had average adjusted Rand below 0.5. This demonstrates the expected robustness of ABCO in the presence of stochastic volatility.

A further statistic to highlight is the average distance from a predicted change point to a true change point. ABCO has an impressive distance of 0.35 which means almost every predicted change point very close to a true changepoint. While E.Divisive and PELT were similar to static Horseshoe in terms of Rand index, they have much greater prediction-to-true distance, implying many more false positives are predicted. The ability to avoid false positives in this setting makes ABCO well suited for diverse

Table 1: Mean Changes with Stochastic Volatility

Algorithms	Rand Avg.	Adj. Rand Avg.	Avg. Diff.	CP	Avg. Dist. to True
ABCO	0.958 _(0.009)	0.912 _(0.018)	0.36	0.35	
Horseshoe	0.736 _(0.016)	0.528 _(0.032)	1.64	23.78	
E.Divisive	0.774 _(0.012)	0.485 _(0.019)	6.01	58.45	
PELT	0.738 _(0.012)	0.397 _(0.019)	9.55	135.81	
WBS	0.659 _(0.015)	0.326 _(0.022)	111.35	154.25	
BCP	0.678 _(0.013)	0.251 _(0.017)	85.75	96.70	

Rand Avg. measures similarity between predicted partition and true partition; the value ranges between 0 and 1 with 1 being a perfect match. Adjusted Rand corrects Rand for random chance of predicting the correct clustering; the standard error is shown in subscript. Avg. Diff. CP. reflects the average difference between true and predicted number of change points. Avg. Dist. to True measures average distance from a predicted change point to the nearest true change point.

applications. In comparison, the static Horseshoe algorithm is less accurate in predicting the correct number of change points and tends to miss some more subtle change as illustrated by the average difference between the number true and predicted changepoints. This further supports the previous finding in [Kowal *et al.* \(2019\)](#) that the SV(1) model provides better estimation of the true mean, which in this case was piece-wise constant. PELT and WBS assume iid Gaussian errors; as a result, they tend to not perform well under this setting.

Furthermore, within the Bayesian framework, ABCO provides estimates both the local mean and point-wise credible bands. This allows tracking both a constant or varying signal within each cluster. We can see in Figure 2 that the credible bands are able to adapt well to regions of high volatility.

3.2 Detecting Changes in Presence of Outliers

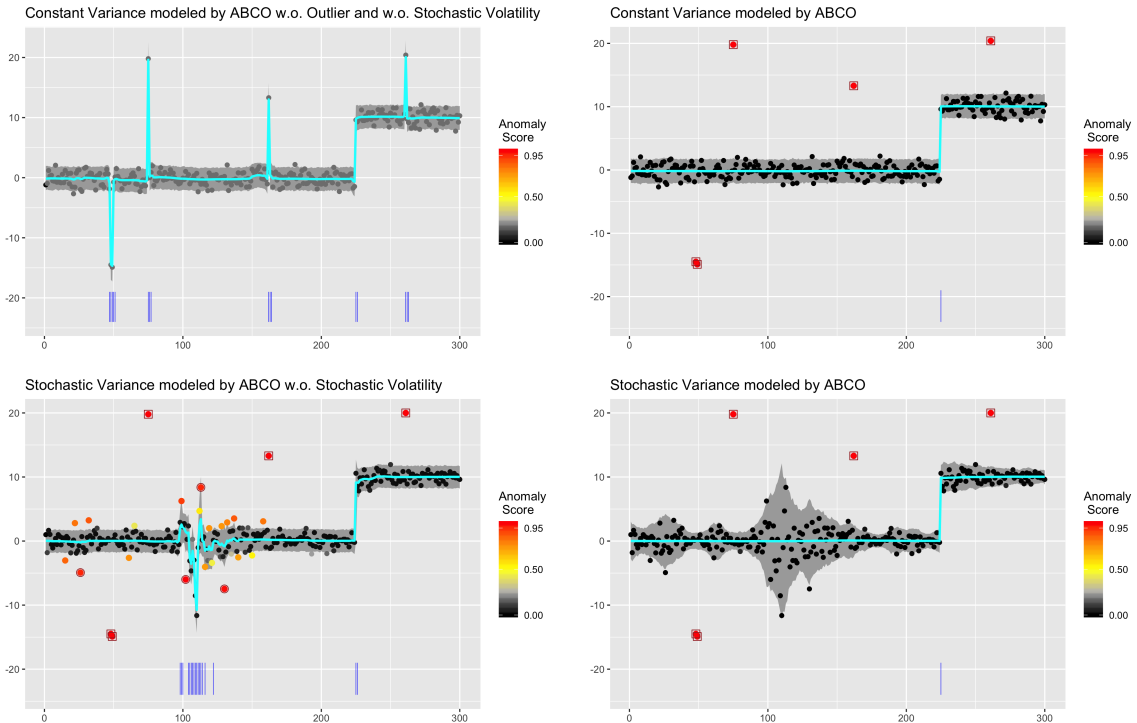
Next we illustrate the effectiveness of ABCO in the presence of significant outliers. Two sets of data are generated: data with changes in mean and data with changes in linear trend. For changes in mean, data sets are generated of length 100-2000, with a single change point approximately 3/4th of the series. The first cluster has mean chosen uniformly at random between 0 and 5 while second cluster has mean chosen uniformly at random between 10 and 15. Both clusters have noise simulated by t-distribution with 5 degrees of freedom. Additionally, significant random outliers are generated within each of the two clusters. We again fit the ABCO model, the static horseshoe model, E.Divisive, PELT, WBS and BCP on the simulated data sets; results are shown in Table 2.

For ABCO, outliers are flagged using the outlier scoring detailed in Section 2.1. We choose a cutoff threshold 0.95 for $\{o_t\}$. Figure 3 shows the effectiveness of local outlier scoring in the presence of stochastic volatility in the ABCO. As shown, modeling stochastic volatility within ABCO increases its effectiveness while maintaining the same level of performance for data sets with constant variance. We hence recommend including both outlier and heteroskedastic noise when deploying ABCO, in general.

For changes in linear trend, data are generated with a length of 100 with a change point randomly

selected in the middle 20% of the data. Linear "meet-up" model is utilized to generate the data, meaning the segments are set to be continuous (end of segment 1 is the same as start of segment 2). The start and end of segment 1 as well as end of segment two are uniformly randomly generated between -100 and 100. The segments are set to have a minimum slope difference of 1.5 to ensure identifiability. Three types of outlier settings are generated: small (5-10 std. dev. away from the true mean), large (25-30 std. dev. away from the true mean) and mixed (5-30 std. dev. away from the true mean). We generate $N = 100$ series for each outlier setting, with 5-10 outliers randomly generated for each segment. Since only the ABCO algorithm can effectively deal with linear trends in presence of outliers, we ran the ABCO algorithm in each of the three settings and reported the results terms of both change point detection accuracy and outlier detection accuracy.

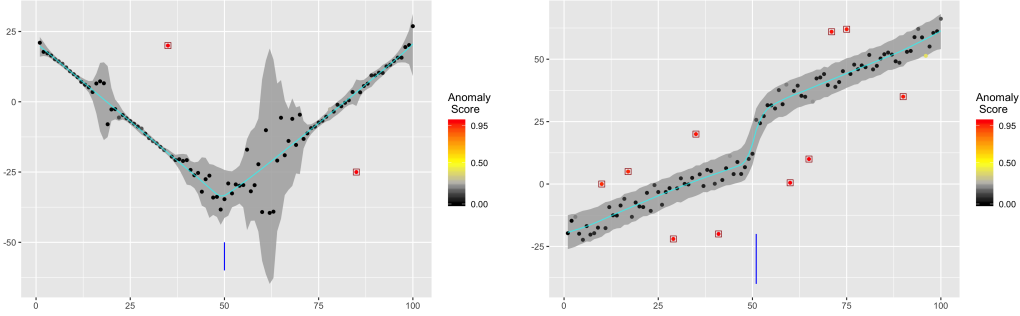
Figure 3: Anomaly Scores with Outliers



The figure illustrates data generated with same signal and outlier but different noise. The top plots are generated with constant variance while the bottom plots are generated with stochastic variance. The top left plot shows results generated by running ABCO model without the outlier component and without stochastic volatility. The bottom left plot shows results generated by running ABCO model without stochastic volatility. As seen in plots above, ABCO struggles to adapt to these datasets without either of the two components. True outliers flagged by the model are highlighted by brown square while false outliers are highlighted by brown circle. Predicted mean is in cyan; predicted change point is shown in blue vertical line and credible bands for data excluding the anomaly term is shown in gray.

The simulation is summarized in Table 2, where it is clear that ABCO again substantially outperforms other models. ABCO consistently achieves an average Rand value of at least 0.974 and an adjusted Rand value around 0.951. This demonstrates the robustness of the ABCO algorithm in dealing with outliers. For distance based algorithms such as E.Divisive and PELT, if the outliers become large enough, they will be treated as change points. A Bayesian algorithm such as BCP, without a clear means to account

Figure 4: Linear Data Examples



Examples of plots generated using simulated data with linear trends, change point and outliers. Left figure shows an example of a linear meet-up model generated with stochastic volatility and 2 outliers. Right figure shows a common linear trend with a jump and outliers. Anomaly scoring is calculated by the ABCO model with true anomalies flagged by brown square. Vertical line indicates predicted change points; cyan line indicates predicted mean with 95 credible bands for signal plus noise in gray.

Table 2: Outlier Extension: Changes in Mean

Algorithms	Rand Avg.	Adj. Rand Avg.	Avg. No. CP	Avg. Dist. to True
ABCO	0.974 _(0.008)	0.951 _(0.015)	1.3	25.51
Horseshoe	0.543 _(0.009)	0.188 _(0.014)	12.0	304.28
E.Divisive	0.822 _(0.014)	0.670 _(0.026)	2.5	102.01
Pelt	0.514 _(0.005)	0.115 _(0.007)	12.1	298.17
WBS	0.575 _(0.008)	0.177 _(0.019)	23.7	286.41
BCP	0.513 _(0.003)	0.173 _(0.005)	21.2	204.89

Result for ABCO against other change point algorithms on simulated data with changes in mean and significant outliers. The metrics are mostly the as those detailed in table 1. Avg. No. CP. measures average number of change points predicted by the algorithm (correct number of change points is 1).

for outliers, also does not work well for on this type of data. Clustered outliers are especially difficult for these algorithms to deal with as they mimic the occurrence of a new cluster and they also break the Gaussian noise assumption. By utilizing a horseshoe plus prior for $\{\zeta_t\}$, ABCO is able to adapt to large outliers that significantly deviate from the data and not treat bursts of outliers as change points.

In the linear trend example, we illustrate the effectiveness of ABCO in flagging locations of outliers in the data. By using the local outlier scoring metric proposed in Section 2.1, ABCO is able to have a high true positive rate and a low false positive rate for all three types of outliers (an example of outlier scoring is seen in figure 4). As seen in table 3, the ABCO algorithm is able to maintain an average Rand value of at least 0.951, signaling its effectiveness in identifying true change points. The detection of both change

Table 3: Outlier Extension: Linear Trends

Algorithms	Outlier Type	Rand Avg.	Adj. Rand Avg.	True Positive Rate	False Positive Rate
ABCO	Small	0.963	0.923	0.751	0.002
	Large	0.951	0.903	0.961	0.007
	Mixed	0.974	0.948	0.943	0.003

Result for ABCO on predicting both change points and outliers in linear settings. Rand and adjusted Rand reflect accuracy of change point detection while true positive rate and false positive rate measures accuracy of outlier detection.

points and outliers simultaneously allows ABCO to provide more information for analysis. As we can see in figure 4, a series may contain a significant amount of outliers, a very difficult or impossible setting for other changepoint algorithm. The ability to incorporate both heteroskedastic noise and outlier detection makes ABCO very widely applicable.

4 Applications

4.1 Amazon Cloudwatch Server Metrics

For our first illustrative application we consider time series from the Numenta Anomaly Benchmark ([Ahmad et al., 2017](#)). Each series considers CPU utilization server metrics on Amazon Cloudwatch, and contains both changepoints and anomalies. Figure 5 illustrates two such series, and two more are shown in Appendix 6.4. Each series exhibits changes in trend, local and global anomalies, and non-constant volatility, and nicely highlights the utility and robustness of ABCO. We also compare ABCO estimates with both WBS and PELT in terms of change points and trend estimation.

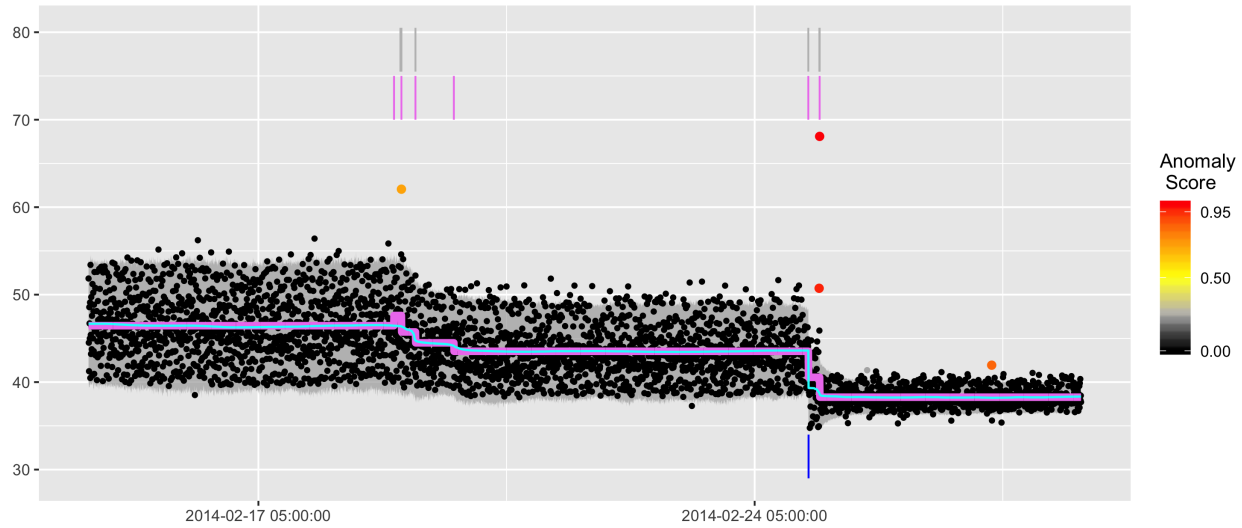
As shown in Figure 5, ABCO performs well in this complicated setting. Both PELT and WBS tend to over-predict the number of change points in the dataset and chase significant point anomalies. As seen in the top plot, ABCO differentiates gradual shifts in mean from abrupt change points. PELT and WBS over-predict change points in regions where there are slight changes in trend. ABCO’s local adaptability effectively handles such features without over-predict the number of change point. Additionally, ABCO is very robust to the presence of potential outliers, whereas extreme outliers force both PELT and WBS to explain them as changepoints. ABCO estimates an outlier signal to model them effectively without affecting the underlying trend model. As seen in Figure 5, in the presence of significant outliers, both WBS and PELT predict an additional changepoint in the second half of the top series and in the first half of the bottom series. This example highlights ABCO’s ability to adapt to real world data and predict true change points without over-predicting in presence of outliers or smooth local trends.

4.2 Global Land Surface Air Temperature

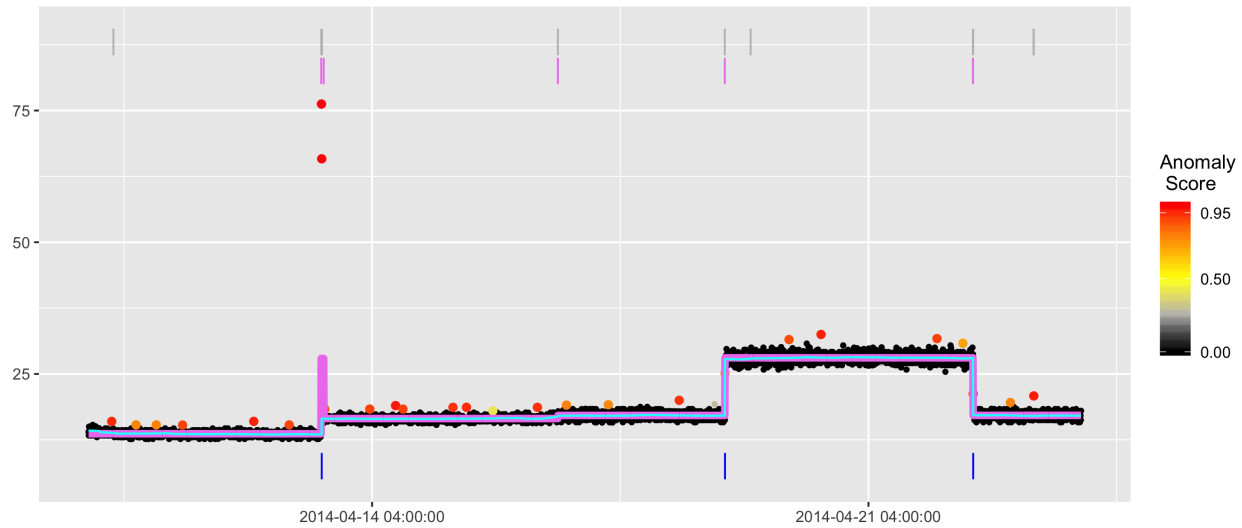
For another illustrative application we consider monthly global land surface air temperature from 1880 to 2018. The data is made available on National Aeronautics and Space Administration website and has been previously analyzed ([Yang and Song, 2014](#)). Identifying changes in climate patterns has become an urgent area of analysis ([Alley et al., 2003](#)). Understanding when the underlying dynamics of global temperature pattern shifts can be very important in policy decision making. The top panel in Figure 6 shows the recorded global land surface air temperature. As shown, there are clear long term linear time trends underlying local annual trends in the data. Overall global temperature appear increasing over time; however, three features make standard change point analysis difficult. First, there exists seasonal

Figure 5: AWS CPU Utilization Results

Amazon Cloudwatch Service CPU Utilization 1



Amazon Cloudwatch Service CPU Utilization 2



Figures show two AWS CPU utilization series with estimates from ABCO, WBS and PELT. The cyan line represents predicted signal from the ABCO algorithm and purple line represents predicted mean from PELT. Change points from the ABCO are shown by blue vertical bars below the series; change points from PELT and WBS are shown by purple and gray vertical bars, respectively, above the series. Dark gray bands represents credible bands produced by ABCO of signal plus noise, which are especially relevant for ABCO local outlier scoring, which is indicated by observation shading.

fluctuation in the data, and these seem somewhat irregular. This implies the local trend is not flat but rather a smooth curve fluctuating through the months. Second, there is differing levels of variability over time. Third, there may be anomalies throughout the data as a result of certain global events.

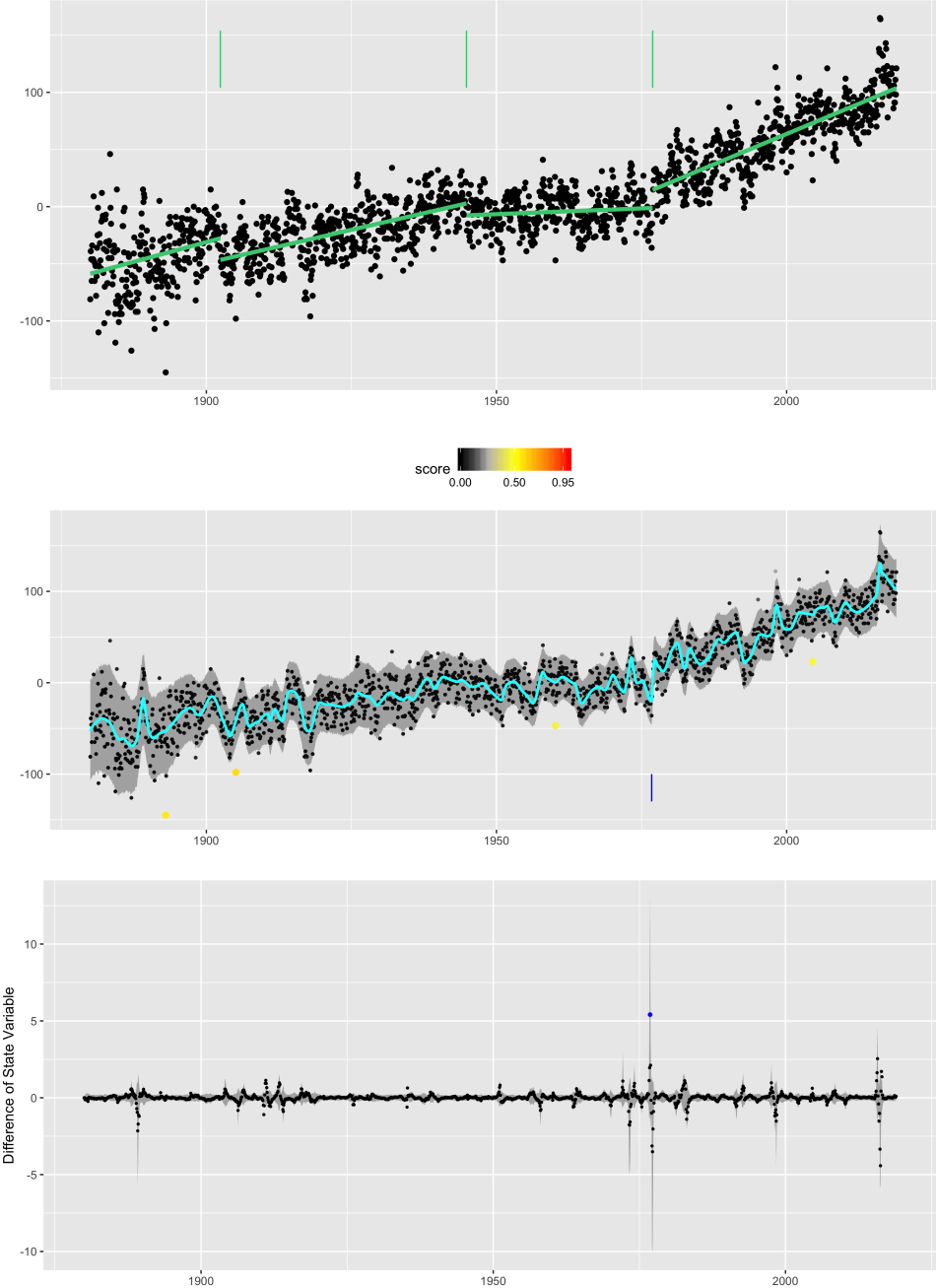
We contrast the results of ABCO with those from the R package `strucchange` ([Zeileis *et al.*, 2002](#)). `Strucchange` estimates structural change in linear regression through a generalized fluctuation test. In addition, we ran PELT and WBS on the first degree difference of the observations, but found no changepoints. For a linear meet-up model, using first degree difference to predict changepoints seems to be a difficult task. With ABCO, we find one changepoint around the year 1976, after which there is a steeper long term slope. In comparison, the `strucchange` algorithm finds 3 change points. This reflects important difference between `strucchange` and ABCO. `Strucchange` attempts to fit piecewise linear trend throughout the series but cannot account for small fluctuations over time, such as seasonal patterns. As seen in the trend estimate from ABCO, the underlying signal fluctuates over time as a result of irregular cyclical patterns over the years that have less variability than the longer term approximately linear lime trends. ABCO is able to model these small fluctuations without predicting them as changepoints.

5 Conclusion

We have proposed an adaptive Bayesian changepoint model with the ability to detect multiple change points within a time series. The model separates the data at each time-step into a trend component, an outlier component and a noise component. For trend estimation with breaks, a horseshoe-like shrinkage is placed on the D th difference of the trend component through a threshold stochastic volatility model with Z -distributed innovations. This shrinkage ensures most increments are relatively small or even nearly zero while allowing some isolated changes to be significantly large. The threshold variable is used to classify large changes as change points. For the outlier component, a horseshoe-plus prior is utilized to model extreme values in the data. For the noise component, a stochastic volatility model is specified to adapt both change and outlier detection to regions of both high and low volatility, whether stochastic or not. Together, all three components allow great flexible adaptive trend modeling, change detection, and outlier scoring.

Through simulation experiments and illustrative applications we have highlighted the unique strengths of ABCO and shown settings where it outperform competing methods, i.e. changepoint series with significant outliers and/or non-constant variance. With a Bayesian framework, ABCO provides a reliable means for assessing changepoints and scoring anomalies, and it can also be further extended, as we demonstrated in interrupted time series analysis and dynamic regression specifications. Further directions include analysis of multivariate series and incorporating covariates into change and outlier detection equations.

Figure 6: Monthly Global Land Surface Air Temperature



The top panel shows the recorded monthly global land surface air temperature from 1880 to 2018 along with predicted change points and estimated trend from the `strucchange` R package (shown in green). The middle panel shows result of running ABCO on the temperature series. Change points found by `strucchange` and ABCO are shown in green and blue vertical bars, respectively. Dark gray credible bands for the signal plus noise are produced by ABCO with the cyan line representing the local mean trend predicted by ABCO. Outlier scoring is also calculated by ABCO and indicated by observations color, in this case with four yellow observations. The bottom panel shows the posterior mean and 80% credible bands for the trend increments (second differences) $\{\omega_t\}$ from ABCO. Here we see ABCO's local adaptivity in allowing $\{\omega_t\}$ to occasionally change slightly over time to account for local fluctuations in the data. But only the highest point (blue) is a change significant enough to be identified as a change point by ABCO.

References

Adams, R. P., and MacKay, D. J. (2007). “Bayesian online changepoint detection,” *Machine Learning* .

Ahmad, S., Lavin, A., Purdy, S., and Agha, Z. (2017). “Unsupervised real-time anomaly detection for streaming data,” *Neurocomputing* **262**, 134–147.

Alley, R. B., Marotzke, J., Nordhaus, W. D., Overpeck, J. T., Peteet, D. M., Pielke, R., and et al. (2003). “Abrupt climate change,” *Science* **299**, 2005–2010.

Aminikhanghahi, S., and Cook, D. J. (2017). “A survey of methods for time series change point detection,” *Knowl Inf Syst*. **51**, 339–367.

Barone-Adesi, F., Gasparrini, A., Vizzini, L., Merletti, F., and Richiardi, L. (2011). “Effects of italian smoking regulation on rates of hospital admission for acute coronary events: a country-wide study,” *PLoS One* **6**.

Bernal, J. L., Cummins, S., and Gasparrini, A. (2017). “Interrupted time series regression for the evaluation of public health interventions: a tutorial,” *International Journal of Epidemiology* **46**, 348–355.

Bhadra, A., Datta, J., Polson, N. G., and Willard, B. (2017). “The horseshoe+ estimator for ultra sparse signals,” *Bayesian Analysis* **12**, 1105–1131.

Braun, J., Braun, R., and Müller, H.-G. (2000). “Multiple changepoint fitting via quasilikelihood, with application to dna sequence segmentation,” *Biometrika* **87**, 301–314.

Carvalho, C. M., Polson, N. G., and Scott, J. G. (2009). “Handling sparsity via the horseshoe,” *AISTATS* **5**, 73–80.

Chen, G., Lu, G., Shang, W., and Xie, Z. (2019). “Automated change-point detection of eeg signals based on structural time-series analysis,” *IEEE Access* **7**.

Chen, J., and Gupta, A. (1997). “Testing and locating variance changepoints with application to stock prices,” *Journal of American Statistics Association* **92**, 739–747.

Cho, H., and Fryzlewicz, P. (2015). “Multiple-change-point detection for high dimensional time series via sparsified binary segmentation,” *J. R. Statist. Soc. B* **77**, 475–507.

Ebrahimzadeh, Z., Zheng, M., Karakas, S., and Kleinberg, S. (2019). “Pyramid recurrent neural networks for multi-scale change-point detection,” .

Erdman, C., and Emerson, J. W. (2008). “A fast bayesian change point analysis for the segmentation of microarray data,” *Bioinformatics* **24**, 2143–2148.

Fearnhead, P., and Rigaill, G. (2017). “Changepoint detection in the presence of outliers,” *Journal of American Statistical Association* **114**, 169–183.

Fryzlewicz, P. (2014). “Wild binary segmentation for multiple change-point detection,” *Annals of Statistics* **42**, 2243–2281.

Giordani, P., Kohn, R., and Dijk, D. v. (2007). “A unified approach to nonlinearity, structural change, and outliers,” *Journal of Econometrics* **137**, 112–133.

Hosszejni, D., and Kastner, G. (2019). “Modeling univariate and multivariate stochastic volatility in r with stochvol and factorstochvol,” .

James, N. A., and Matteson, D. S. (2014). “ecp: An r package for nonparametric multiple change point analysis of multivariate data,” *Journal of Statistical Software* **62**.

Kastner, G., and Frühwirth-Schnatter, S. (2014). “Ancillarity-sufficiency interweaving strategy (asis) for boosting mcmc estimation of stochastic volatility models,” *Computational Statistics and Data Analysis* **76**, 408–423.

Kawahara, Y., Yairi, T., and Machida, K. (2007). “Change-point detection in time-series data based on subspace identification,” *7th IEEE International Conference on Data Mining* 559–564.

Killick, R., Fearnhead, P., and Eckley, I. (2012). “Optimal detection of changepoints with a linear computational cost,” *Journal of American Statistical Association* **107**, 1590–1598.

Kim, S., Shephard, N., and Chib, S. (1998). “Stochastic volatility: Likelihood inference and comparison with arch models,” *Review of Economic Studies* **65**, 361–393.

Kowal, D., Matteson, D., and Ruppert, D. (2019). “Dynamic shrinkage process,” *J. R. Statist. Soc. B* **81**.

Liu, S., Yamada, M., Collier, N., and Sugiyama, M. (2013). “Change-point detection in time-series data by relative density-ratio estimation,” *Neural Networks* **43**, 72–83.

Makalic, E., and Schmidt, D. F. (2016). “A simple sampler for the horseshoe estimator,” *IEEE Signal Processing Letters* **23**.

Matteson, D. S., and James, N. A. (2014). “A nonparametric approach for multiple change point analysis of multivariate data,” *Journal of the American Statistical Association* **109**, 334–345.

Mccausland, W., Miller, S., and Pelletier, D. (2011). “Simulation smoothing for state-space models: A computational efficiency analysis,” *Computational Statistics and Data Analysis* **55**, 199–212.

Montanez, G. D., Amizadeh, S., and Laptev, N. (2015). “Inertial hidden markov models: Modeling change in multivariate time series,” *AAAI* 1819–1825.

Nakajima, J., and West, M. (2013). “Bayesian analysis of latent threshold dynamic models,” *Journal of Business and Economic Statistics* **31**, 151–164.

Neil, R. (2003). “Slice sampling,” *The Annals of Statistics* **31**, 705–767.

Omori, Y., Chib, S., Shephard, N., and Nakajima, J. (2007). “Stochastic volatility with leverage: Fast and efficient likelihood inference,” *Journal of Econometrics* **140**, 425–449.

Polson, N. G., Scott, J. G., and Windle, J. (2013). “Bayesian inference for logistic models using polya–gamma latent variables,” *Journal of the American Statistical Association* **108**, 1339–1349.

Rehman, M. H. u., Liew, C. S., Abbas, A., Jayaraman, P. P., Wah, T. Y., and Khan, S. U. (2016). “Big data reduction methods: A survey,” *Data Sci. Eng.* **1**, 265–284.

Ritter, C., and Tanner, M. A. (1992). “Facilitating the gibbs sampler: The gibbs stopper and the griddy-gibbs sampler,” *Journal of the American Statistical Association* **87**, 861–868.

Saatçi, Y., Turner, R., and Rasmussen, C. E. (2010). “Gaussian process change point models,” *ICML 10 Proceedings of the 27th International Conference on International Conference on Machine Learning* 927–934.

Serumaga, B., Ross-Degnan, D., Avery, T., Elliott, R., Majumdar, S. R., Zhang, F., and Soumerai, S. (2011). “Effect of pay for performance on the management and outcomes on hypertension in the united kingdom: Interrupted time series study,” *BMJ* **342**.

Solow, A. (1987). “Testing for climate change: An application of the two-phase regression model,” *Journal of Climate and Applied Meteorology* **26**.

Tan, B. A., Gerstoft, P., Yardim, C., and Hodgkiss, W. S. (2015). “Change-point detection for recursive bayesian geoacoustic inversions,” *The Journal of the Acoustical Society of America* **137**, 1962–1970.

Wagner, A. K., Soumerai, S. B., F., Z., and Ross-Degnan, D. (2002). “Segmented regression analysis of interrupted time series studies in medication use research,” *Journal of Clinical Pharmacy and Therapeutics* **27**, 299–309.

Yang, Y., and Song, Q. (2014). “Jump detection in time series nonparametric regression models: a polynomial spline approach,” *Annals of the Institute of Statistical Mathematics* **66**, 325–344.

Zeileis, A., Leisch, F., Hornik, K., and Kleiber, C. (2002). “Strucchange: An r package for testing for structural change in linear regression models,” .

Zhang, W., Gilbert, D., and Matteson, D. S. (2019). “Abacus: Unsupervised multivariate change detection via bayesian source separation,” *Proceedings of the 2019 SIAM International Conference on Data Mining* .

6 Appendix

6.1 MCMC Algorithm Details

In this subsection, we will expand upon the summary of section 2.4 and detail the MCMC sampling algorithm for the rest of the parameters in the ABCO model.

6.1.1 Sampling the log evolution variance $\{h_t\}$

To sample the log evolution variance, we will use a similar sampling method as detailed in [Kastner and Frühwirth-Schnatter \(2014\)](#). In details below, I will describe the setup for $D = 1$; the sampler for $D = 2$ follows a similar idea.

As seen in equation 3, the evolutionary equation is then given by $h_{t+1} = \mu + (\phi_1 + \phi_2 s_t)(h_t - \mu) + \eta_{t+1}$. To sample the log-volatility $\{h_t\}$, we will first define $z_t = \log(\omega_t^2 + c)$. Since each ω_t follows a Gaussian distribution, each ω_t^2 follows a chi-squared distribution. To sample the log of a chi-squared distribution, we use the 10-component discrete mixture approximation given in [Omori et al. \(2007\)](#) due to its computational efficiency. We will rewrite $z_t \stackrel{ind.}{\sim} N(h_t + m_{r_t}, v_{r_t})$, where m_i, v_i for $i=1,..,10$ are mean and variance component indicators. With the discrete mixture components, we can write the joint likelihood for all h_1, \dots, h_T as follows: $\mathbf{z} \sim N(\mathbf{m} + \tilde{\mathbf{h}} - \mathbf{u}, \Sigma_v)$ where $\mathbf{z} = (z_1, \dots, z_T)$, $\mathbf{m} = (m_{r_1}, \dots, m_{r_T})$, $\tilde{\mathbf{h}} = (h_1 - \mu, \dots, h_T - \mu)$, $\mathbf{u} = (\mu_1, \dots, \mu_T)$, and $\Sigma_v = \text{diag}(v_{r_1}, \dots, v_{r_T})$. The evolution equation can be written as $D\tilde{\mathbf{h}} \sim N(\mathbf{0}, \Sigma_\xi)$ where $\Sigma_\xi = \text{diag}(\xi_1, \dots, \xi_T)$, and D is a $T \times T$ matrix with 1 on the diagonal, $(-(\phi_1 + \phi_2 s_1), \dots, -(\phi_1 + \phi_2 s_{T-1}))$ on the first off-diagonal and 0 elsewhere.

With the above setup, we can calculate the parameters of the full conditional distribution for $\tilde{\mathbf{h}}$ using the *all without a loop sampler* detailed in [McCausland et al. \(2011\)](#). The full conditional distribution is given by: $\tilde{\mathbf{h}} \sim N(\mathbf{Q}^{-1}\mathbf{l}, \mathbf{Q}^{-1})$ where \mathbf{Q} is a symmetric tridiagonal matrix with main diagonal entries \mathbf{Q}_0 and off-diagonal entries \mathbf{Q}_1 given by

$$\begin{aligned}\mathbf{Q}_0 &= [(v_{r_1}^{-1} + \xi_1 + (\phi_1 + \phi_2 s_2)^2 \xi_2), \dots, (v_{r_{T-1}}^{-1} + \xi_{T-1} + (\phi_1 + \phi_2 s_T)^2 \xi_T), (v_{r_T}^{-1} + \xi_T)] \\ \mathbf{Q}_1 &= [-(\phi_1 + \phi_2 s_2) \xi_2, -(\phi_1 + \phi_2 s_3) \xi_3, \dots, -(\phi_1 + \phi_2 s_T) \xi_T] \\ \mathbf{l} &= \left[\frac{z - m_{r_1} - \mu}{v_{r_1}}, \frac{z - m_{r_2} - \mu}{v_{r_2}}, \dots, \frac{z - m_{r_T} - \mu}{v_{r_T}} \right]\end{aligned}$$

With the full conditional distribution derived above, we sample $\tilde{\mathbf{h}}$ using the *backhand-substitution method* detailed in [Kastner and Frühwirth-Schnatter \(2014\)](#).

6.1.2 Sampling the volatility parameters μ, ϕ_1, ϕ_2

Since a horseshoe prior is used for the evolution error, we propose the following prior for τ : $\tau \sim C^+(0, \frac{\hat{\sigma}_y}{\sqrt{T}})$ where $\hat{\sigma}_y$ is the standard deviation of the data (y_1, \dots, y_T) . Since $\mu = \log(\tau^2)$, using Pólya-Gamma mixing

parameter as seen in [Polson *et al.* \(2013\)](#), the prior for μ is given by: $[\mu | \hat{\sigma}_y, \tau] \sim N(\log(\frac{\hat{\sigma}_y^2}{T}), \xi_\mu^{-1})$, where $\xi_\mu \sim PG(0, 1)$. Given that $h_1 \sim N(\mu, \xi_0^{-1})$ where $\xi_0 \sim PG(0, 1)$, the full conditional distribution for μ can be derived from formula for conjugate normal prior. The full conditional distribution is given by: $\mu \sim N(Q_\mu^{-1}l_\mu, Q_\mu^{-1})$, where

$$Q_\mu = \xi_\mu + \xi_0 + \sum_{t=1}^{T-1} (1 - \phi_1 - \phi_2 s_t) \xi_t$$

$$l_\mu = \xi_\mu \log(\frac{\sigma_\epsilon^2}{T}) + \xi_0 h_1 + \sum_{t=1}^{T-1} (1 - \phi_1 - \phi_2 s_t) (h_{t+1} - (\phi_1 + \phi_2 s_t) h_t)$$

For ϕ_1 , assume a prior $\frac{\phi_1+1}{2} \sim \text{Beta}(10, 2)$, which restricts $|\phi_1| \leq 1$. The full conditional distribution is then sampled using slice sampler with a lower limit of 0 and a upper limit of 1 ([Neil, 2003](#)). Slice sampling provide an effectively way to sample a distribution with known lower and upper limit. The full conditional is given by:

$$f_{(\phi_1+1)/2}(x) = [-\frac{1}{2} \sum_{t=1}^{T-1} (\tilde{h}_{t+1} - (2x - 1 + \phi_2 s_t) \tilde{h}_t)^2] + \text{dBeta}(x, 10, 2)$$

where $\text{dBeta}(x, 10, 2)$ is the pdf of the beta distribution with parameters $\alpha = 10$ and $\beta = 2$.

For ϕ_2 , we assume a prior of truncated normal distribution with lower bound of 0. $\phi_2 \sim N(-2, 0.5) \mathbf{1}_{\phi_2 \leq 0}$. We restricts ϕ_2 to be negative as ϕ_2 functions as a negative buffer after discovering a change point. The full conditional can be calculated by define $\mathbf{s} = \{t; s_t = 1\}$; it is given by:

$$f_{\phi_2}(x) = [-\frac{1}{2} \sum_{t \in \mathbf{s}} (\tilde{h}_{t+1} - (\phi_1 + x s_t) \tilde{h}_t)^2] + \text{dNorm}(x, -2, 0.5)$$

where $\text{dNorm}(x, -2, 0.5)$ is the pdf of the normal distribution with mean -2 and standard deviation of 0.5 . The full conditional distribution is sampled with upper limit of 0.

6.1.3 Sampling the rest of parameters

The evolution error $\{\eta_t\}$ is defined by a Pólya-Gamma mixing parameter ([Polson *et al.* \(2013\)](#)) given by $[\eta_t | \xi_t] \stackrel{ind.}{\sim} N(0, \xi_t^{-1})$ where $\xi_t^{-1} \sim PG(1, 0)$. The Pólya-Gamma mixing parameters, $\{\xi_t\}$, are sampled using the `rpg()` function from `Bayeslogic` package. The full conditional distribution is given by: $[\xi_t | \eta_t] \sim PG(1, \tilde{h}_t - (\phi_1 + \phi_2 s_{t-1}) (\tilde{h}_{t-1}))$. The discrete mixture indicators r_t are sampled in the same manner as in [Kim *et al.* \(1998\)](#). Next, the state variable $\{\beta_t\}$ is sampled in a similar manner as in [Kowal *et al.* \(2019\)](#). Lastly, the observation variance ϵ_t follow a standard stochastic volatility model. The observational variances are sampled using `stochvol` package.

6.2 Changepoints in Dynamic Regression

Given the Bayesian framework, the model can be extended to the case for multiple predictors. This is an extension to allow for identification of change points within a regression problem. Let $\mathbf{x}_t = (x_{1,t}, \dots, x_{p,t})$ be p predictors for y at time t , the model can be written as follows:

$$y_t = \mathbf{x}'_t \boldsymbol{\beta}_t + \zeta_t + \epsilon_t \quad (5)$$

$$\Delta^D \beta_{t+1} = \boldsymbol{\omega}_t \quad \omega_{j,t} \sim N(0, \tau_{\omega,0}^2 \tau_{\omega,j}^2 \lambda_{\omega,j,t}^2) \quad (6)$$

where $\tau_{\omega,0}$ is the global shrinkage parameter and $\tau_{\omega,j}$ is the shrinkage associated with each predictor.

The evolution equation can be written as follows:

$$\mathbf{h}_{t+1} = \boldsymbol{\mu} + (\boldsymbol{\phi}_1 + \boldsymbol{\phi}_2 \mathbf{s}_t) (\mathbf{h}_t - \boldsymbol{\mu}) + \boldsymbol{\eta}_{t+1} \quad (7)$$

In the above equation, $\mathbf{h}_{t+1} = (h_{1,t+1}, \dots, h_{p,t+1})$, $\boldsymbol{\phi}_1 = (\phi_{1,1}, \dots, \phi_{p,1})$, $\boldsymbol{\phi}_2 = (\phi_{1,2}, \dots, \phi_{p,2})$, $\boldsymbol{\mu} = (\mu_1, \dots, \mu_p)$ and $\mathbf{s}_t = (s_{1,t}, \dots, s_{p,t})$. Each $s_{i,t}$ for $i = 1, \dots, p$ can be written as follows:

$$s_{i,t} = \begin{cases} 1 & \text{if } \log(\omega_{i,t}^2) > \gamma_i \\ 0 & \text{if } \log(\omega_{i,t}^2) \leq \gamma_i \end{cases}$$

The idea for the regression extension is finding a threshold level γ_i for each of the predictors and evaluate change point within each predictors separately. For MCMC simulations, each threshold level γ_i will be evaluated conditional on all other threshold levels. For the most part, the same sampling scheme is used for the multivariate case as the univariate case.

6.3 Additional Simulations

Rand index measures similarity between two different clustering of the data sets. Let X denote a clustering given by the model and let Y denote the true clustering of the data. All pairs of points can then divided into four groups: pairs that are placed in same cluster in X and in same cluster in Y (A); pairs that are placed in same cluster in X and in different clusters in Y (B); pairs that are placed in different clusters in X and in same cluster in Y (C); pairs that are placed in different clusters in X and in different clusters in Y (D). Rand index is calculated as $\frac{A+D}{A+B+C+D}$. Adjusted rand index corrects for random chance that pairs of points will be placed together. We chose Rand index and adjusted Rand index as they give good measurement of similarity between the predicted clusters and the true clusters.

Figure 7: Example Plots for Quadratic Trend with One Change Point

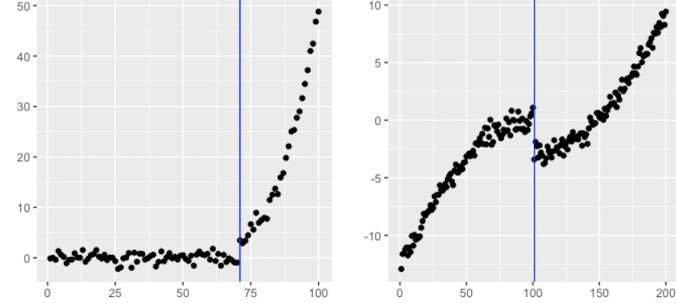


Table 4: Quadratic Trend with One Change Point

Algorithms	Data Length	Rand Avg.	Adj. Rand Avg.	Avg. No. CP	No. 0 CP	Avg. Dist. to True	Standard Error
ABCO	100	0.977	0.952	1.09	4	0.20	0.020
	200	0.998	0.996	1.13	0	0.17	0.001
	400	0.998	0.995	1.19	0	0.21	0.002
Horseshoe	100	0.821	0.628	1.39	33	1.48	0.044
	200	0.829	0.639	1.32	32	2.88	0.044
	400	0.831	0.637	1.41	33	2.29	0.045

Avg. No. CP is the average number of change points predicted per simulation. No. 0 CP is the number of simulations out of 100 which zero change points are predicted; this acts as an indicator on how likely the algorithm will under-predict in quadratic trends.

6.3.1 Quadratic Trends

Another advantage of the Bayesian framework is the ability to detect quadratic trends. The flexibility of the framework allows us to change to perform 3rd degree difference on the data. Additionally, since quadratic trends are similar to linear trends on a local scale, setting $D=3$ can successfully detect quadratic trends. In the results below, we show simulation results of ABCO versus the horseshoe model in quadratic trends.

For the simulation, we simulated data of length 100, 200, and 400 to test the robustness of the algorithm to length of data sets. We generated data sets that has one change point. 100 data sets are generated for each length. The change point is selected at random between the middle 50th percentile of the data. The change point segments the data into two clusters; each cluster has a random start mean ranging from follows for the formula of $ax^2 + bx + c$, where a, b, c are random integers ranging from -20 to 20. We also added a gaussian noise of 1 to the model. The mean results from the simulations for the ABCO model versus the horseshoe model are detailed below. We skipped the E-divisive, PELT, WBS and BCP algorithms as they are not intended to detect these type of changes and running the algorithms on second degree difference of the data give poor results. See Figure 6 for some examples of simulated data.

Looking at the results from table 5, once again ABCO is shown to outperform the horseshoe model in terms of higher order trends. From the results of simulations, ABCO is able to average a Rand value of around 0.99 across multiple data length and adjusted Rand of at least 0.95. This demonstrate that ABCO is able to consistently detect the correct change point location. Looking at the average number of

Table 5: Multivariate Simulation with Three Predictors

Algorithms	Data Length	Rand Avg.	Adj. Rand Avg.	Avg. No. CP Pred1	Avg. No. CP Pred2	Avg. No. CP Pred3
ABCO	100	0.9966	0.9928	2.34	0	0
	200	0.9932	0.9856	2.44	0	0
	400	0.9846	0.9665	2.67	0	0

Avg. No. CP Pred1 measures on average how many change points are predicted in the coefficients for predictor 1. Avg. No. CP Pred2 measures on average how many change points are predicted in the coefficients for predictor 2. Avg. No. CP Pred3 measures on average how many change points are predicted in the coefficients for predictor 3.

change points predicted; the ABCO model predicts on average around 1 change points. The Horseshoe model performs a bit worse as it tends to miss some subtle changes and over-predict in others cases. Looking at the number of simulations with zero change point predicted, the Horseshoe model on average, predict zero change point on one-third of the simulation. ABCO is much better at not under-predicting. Furthermore, the ABCO model has much smaller standard errors in comparison to the horseshoe model. This further illustrates the consistency of the ABCO algorithm.

6.3.2 Regression Simulation

For regression simulations, the goal is to test the ability for the ABCO to detect changes in the "true" predictors. We simulated 100 data sets of length 100, 200, 400 with Gaussian noise of 1. For each dataset, we generate three predictors ($\mathbf{x}_t = [x_{1t}, x_{2t}, x_{3t}]$): the first predictor ($\{x_{1t}\}$) will be a vector of 1s; the second predictor ($\{x_{2t}\}$) and the third predictor ($\{x_{3t}\}$) are just random Gaussian noises. For the time-varying coefficient matrix $\{\beta_t\}$, the coefficients for the first predictor has a jump (two change points) in the middle 50th percentile of the data while the coefficients for the second and third predictors are random noises. The response variable is generated as:

$$y_t = \mathbf{x}_t' \beta_t + \epsilon_t \quad \epsilon_t \sim N(0, 1)$$

With the multivariate simulation, we only ran the ABCO on the data as most other change point algorithms are not designed for regression setting. For each simulation, we calculated the average rand and adjusted rand for each of the three predictors as well as the average number of change points predicted for each predictor. The results are seen in table 5.

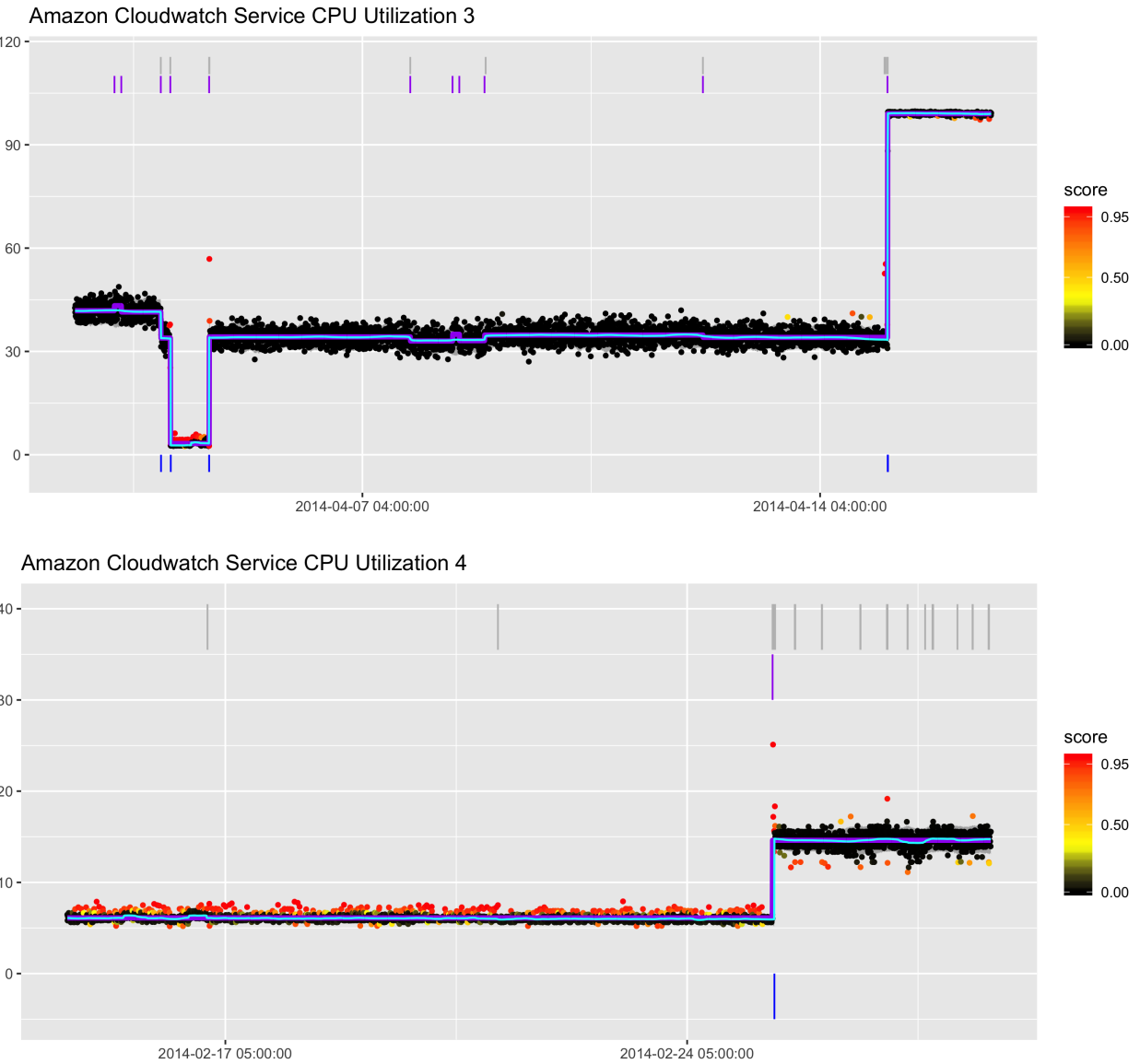
As seen in the table 5, the ABCO algorithm is very accurate for multivariate examples. The algorithm is able to detect only change points in the coefficients true predictor (predictor 1) while detecting no change points in the random noise predictors. The ability to place the changes in the true $\{\beta_t\}$ can be very useful for analyzing which predictor leads to changes in the response variable. Through various data length, the algorithm consistently achieves an average adjusted rand value of above 0.95, showing it can consistently detect the true location of change points.

6.4 Additional Real World Analysis

6.4.1 Amazon Cloudwatch Server Metrics

Figure 7 illustrates results from running ABCO, PELT and BCP on two additional data of CPU utilization server metrics on Amazon Cloudwatch. Just like in the previous two examples in section 4.2, ABCO predicts the least number of change points in comparison to PELT and BCP as ABCO does not chase outliers. As seen in plot for Amazon Cloudwatch Service CPU Utilization 3, ABCO does the best job at not predicting regions with high outliers as change points and not predicting change points at subtle shifts in mean in the middle region of the data.

Figure 8: AWS CPU Utilization Additional Results



Figures show two more examples of results on ABCO, WBS and PELT on AWS CPU utilization dataset. The cyan line represents predicted signal from the ABCO algorithm and purple line represents predicted mean from PELT. Change points from the ABCO are shown by blue vertical bars; change points from PELT are shown by purple vertical bars and change points from WBS are shown by gray vertical bars. Dark gray bands represents credible bands produced by ABCO of signal plus noise.